JCTC Journal of Chemical Theory and Computation

Modeling Charge Resonance in Cationic Molecular Clusters: Combining DFT-Tight Binding with Configuration Interaction

Mathias Rapacioli,* Fernand Spiegelman, Anthony Scemama, and André Mirtschink

Université de Toulouse, UPS, LCPQ (Laboratoire de Chimie et Physique Quantiques), IRSAMC, 118 Route de Narbonne, F-31062 Toulouse, France, and CNRS, LCPQ (Laboratoire de Chimie et Physique Quantiques), IRSAMC, F-31062 Toulouse, France

Received July 23, 2010

Abstract: In order to investigate charge resonance situations in molecular complexes, Wu et al. (*J. Chem. Phys.* **2007**, *127*, 164119) recently proposed a configuration interaction method with a valence bond-like multiconfigurational basis obtained from constrained DFT calculations. We adapt this method to the Self-Consistent Charge Density-Functional-based Tight Binding (SCC-DFTB) approach and provide expressions for the gradients of the energy with respect to the nuclear coordinates. It is shown that the method corrects the wrong SCC-DFTB behavior of the potential energy surface in the dissociation regions. This scheme is applied to determine the structural and stability properties of positively charged molecular dimers with full structural optimization, namely, the benzene dimer cation and the water dimer cation. The method yields binding energies in good agreement with experimental data and high-level reference calculations.

1. Introduction

The description of neutral molecular clusters requires the consideration of various contributions of the intermolecular energy, including Pauli repulsion, polarization, electrostatics (static multipole interactions), induction forces (multipole-induced multipole interactions), and London dispersion. The treatment of the electronic structure of singly ionized molecular clusters also needs to consider charge resonance, which may cause the charge to be partially or totally delocalized over the molecular units and polarization contributions due to the influence of the charge. Both lead to a stabilization of the charged species as compared to the analogous neutrals. A proper description requires correct balance between charge delocalization and polarization forces.

While Density Functional Theory (DFT) is an appealing method for describing the electronic properties of clusters with dozens, maybe hundreds, of atoms, at least in single point calculations, most common functionals are known to fail in properly describing dispersion forces. This is the first handicap to deal with by treating molecular clusters. The search for new functionals accounting for dispersion[1−9] (for a review, see ref 10) is a very active field, while semiempirical corrections to standard DFT calculations are also used.[11−18] The description of charge resonance in molecular clusters is another serious problem in standard density functional approaches. Using the Kohn−Sham formalism with these functionals, one arising problem is due to the self-interaction of the delocalized charge. Many investigations have addressed the analysis and correction of the self-interaction error arising with approximated DFT functionals (see, for instance, refs 19−38). This error is particularly prevalent in the dissociation of radical cations.[35,36] Similarly, a cationic molecular dimer involving two identical units should dissociate into one molecular cation and one neutral, but in a restricted DFT scheme, the charge is asymptotically equally shared by the two units, breaking the energy additivity and further introducing a spurious Coulomb interaction between the two moieties. Although such an artifact is essential in the dissociation, it is also expected to play a role all over the potential energy surface, including the equilibrium geometries.

* To whom correspondence should be addressed. E-mail: mathias.rapacioli@irsamc.ups-tlse.fr.

10.1021/ct100412f
Published on Web 12/13/2010

A correct description of dissociation is in principle easily obtained by the use of a multiconfigurational wave function. It can be achieved by high-level methods like Configuration Interaction[39,40] (CI)-based methods (Multi-Configurational Self-Consistent Field,[41] MCSCF; Multi-Reference Configuration Interaction,[42] MRCI) or Coupled Cluster[43] (CC) approaches (for a review, see ref 44) but at a high computational cost. Such calculations may provide benchmarks on reasonably small systems (essentially dimers) but rapidly exceed today's possibilities as soon as the molecular units exceed a few tens of atoms.

One of the tracks for circumventing the drawbacks of the present state DFT in an *ab initio* framework is to combine CI, for describing long-range (lr) electron−electron interactions, and DFT, for the short-range electron−electron interactions (sr). This gave rise to the lr−sr formalism following Savin's formulation,[45−48] enabling combinations of Møller−Plesset (MP) perturbation,[49−51] CC, and/or CI approaches with DFT. This formulation is quite attractive; nevertheless, its numerical cost is significantly larger than that of a standard DFT calculation.

Alternatively, charge resonance (or excitation resonance) is described quite simply in valence bond-like approaches[52−55] by explicitly considering the multiconfigurational nature of the wave function via the definition of a basis arising from configurations in which the charge (or excitation) is localized on a given fragment of the system. This is the essence of the excitonic models originating from solid state physics (see for instance ref 56 and references therein) but also used in molecular materials and even biological systems. An application to cationic molecular clusters of polycyclic aromatic hydrocarbon (PAH) was published by Bouvier et al.,[57] defining a resonance charge model based on frozen molecules and parametrized from *ab initio* CI calculations on dimers. Diatomics-in-molecule modeling of singly ionized rare gas clusters can also be expressed in a valence bond picture with a basis of atom-localized hole configurations and no internal geometrical structure.[58−60] That paved the way for extensive simulations of the electronic and dynamical properties of ionized rare gas clusters (see for instance Calvo et al.[61,62]).

More recently, the concept of a valence bond configuration description in a DFT framework was proposed by the group of Van Voorhis et al.[63−69] to investigate charge delocalization in mixed valence compounds exhibiting possible bistability with the perspective of controlling charge transfer. They developed a method combining Constrained DFT,[63−65] used to build charge localized configurations, with a small CI-like scheme (CDFT-CI) to deal with charge delocalization in extended systems. From the computational point of view, it is extremely appealing for singly charged clusters, since the static correlation associated with charge resonance is treated by the CI-like scheme, which in this case is linear scaling (as would be complete active space self-consistent field CASSCF[70] with a single hole in the MOs resulting from the HOMOs of the individual molecules), and the dynamical correlation is treated at the DFT level in a single configuration scheme (whereas a CASSCF would need complementing with dynamical correlation, for instance, CASPT2[71]). For addressing large systems, Self-Consistent-Charge Density-Functional-based Tight Binding (SCC-DFTB)[72−75] is interesting since it is computationally faster than DFT. It is derived from DFT through several approximations allowing the use of tabulated overlap and interaction integrals.

As SCC-DFTB is derived from DFT, it also inherits its lack of describing charge resonance with standard functionals essentially due to the self-interaction error. Detailed analysis of this problem in DFT proposals for self-interaction free functionals were given by Grafenstein et al.[35,36,76] Interestingly, some of those schemes produce localized orbitals. The transfer of such a concept within the DFTB framework would certainly be of interest. However, self-interaction corrections should introduce many centers' contributions into the DFTB parameters representing the Coulomb-exchange-correlation contribution, beyond the two-center approximations for electron−electron interaction integrals, a key point of the DFTB efficiency. This would require analytical assumptions for these terms, further parametrization, and transferability checking.

Recently, we presented a preliminary application of the CDFT-CI method in the SCC-DFTB framework also using approximations to determine the CI couplings. We studied coronene clusters with constrained geometries, because of the lack of gradients.[77] One of the interests of CDFTB-CI is to be safe in regard to all dissociation channels, even multicenter fragmentation.

In the present paper, we present the general adaptation of the CDFT+CI method to the SCC-DFTB framework, with the aim of future investigations of charge resonance in molecular clusters with large sizes. This method is called DFTB-VBCI (Valence Bond CI). In order to perform geometry optimizations, we also derive analytical expressions for the energy gradients with respect to the nuclear coordinates. It allows us to achieve full structural optimization for the benzene dimer and water dimer cations, respectively.

Section 2 is devoted to the presentation of the general methodology, the DFTB-VBCI approach, and the derivation of analytical expressions for the nuclear forces. In section 3, we benchmark the method on ionic benzene and water dimers on the basis of comparisons with high-level calculations. A summary and perspectives are given in section 4.

2. Methodology

The DFTB-VBCI method is an adaptation of the CDFT+CI approach[63−69] to the SCC-DFTB scheme with the aim of treating charge resonance in ionized molecular clusters. In this approach, the wave function of the system Ψ is expressed in a basis $\{\Phi^I\}$ of configurations. For each configuration, the charge is localized on a given fragment of the system. The intuitive decomposition of a molecular cluster leads to identifying the N_{frag} fragments as the monomers, and the wave function becomes

$$\Psi = \sum_{I}^{N_{\mathrm{frag}}} b_I \Phi^I \tag{1}$$

where Φ^I is the configuration where the charge is fully carried by fragment I. Each charge localized configuration Φ^I is a single Slater determinant, built from the molecular

orbitals (MO) $\{\phi_i^I\}$ resulting from a constrained SCC-DFTB calculation. These VB like configurations then interact within a small CI-like scheme, giving their coefficients b_I in the wave function and the ground state energy.

In this methodological part, we first briefly recall the SCC-DFTB scheme basics (section 2.1) before explaining the derivation of the charge localized configurations Φ^I using the constrained SCC-DFTB (section 2.2) and the CI-like scheme calculation (section 2.3). We present then analytical expressions for the nuclear gradients (section 2.4) and some further approximations to accelerate the approach (section 2.5). We adopt different font conventions to distinguish between matrices expressed in different basis sets. For instance, a Hamiltonian matrix is written as H in the atomic orbital (AO) basis set; $\boldsymbol{H}$ in the MO basis set, and $\mathbf{H}$ in the determinant basis set (the basis of the charge-localized configurations).

2.1. DFT and SCC-DFTB. Several reviews on the DFTB and SCC-DFTB methods can be found in the literature.[72−75] SCC-DFTB differs from Kohn−Sham DFT expressed on a local basis set according to the following approximations: (i) The DFT energy is expanded up to the second order with respect to charge density fluctuations around a given reference density. (ii) All three center interaction integrals are neglected as well as two center integrals involving atomic orbitals belonging to the same atom. (iii) The MOs are expressed in a minimal atomic basis set

$$\phi_i = \sum_\mu c_{i\mu}\varphi_\mu \tag{2}$$

(iv) The short distance repulsive potential is expressed as a function of two body interactions. (v) The second-order term in the DFT energy expansion is expressed as a function of atomic Mulliken charges and a Γ matrix. With those approximations, the total SCC-DFTB energy reads

$$E^{\text{SCC-DFTB}} = \sum_{\alpha,\beta\neq\alpha}^{\text{atoms}} E_{\alpha\beta}^{\text{rep}} + \sum_i n_i\langle\phi_i|\hat{H}^0|\phi_i\rangle + \frac{1}{2}\sum_{\alpha,\beta}^{\text{atoms}} \Gamma_{\alpha\beta}q_\alpha q_\beta \tag{3}$$

where $\hat{H}^0$ is the Kohn−Sham operator at the reference density and $E_{\alpha\beta}^{\text{rep}}$ is the repulsive potential between atoms α and β. The matrix elements of $\hat{H}^0$ expressed in the atomic basis set as well as $\Gamma_{\alpha\beta}$ and $E_{\alpha\beta}^{\text{rep}}$ are interpolated from two body DFT calculations. n_i represents the atomic orbital occupation numbers, and q_α represents the atomic Mulliken charges. The energy minimization is obtained by self-consistently solving the secular equation

$$\sum_\nu c_{i\nu}(H_{\mu\nu} - \varepsilon_i S_{\mu\nu}) = 0 \quad \forall\mu, i \tag{4}$$

S is the atomic basis overlap matrix, and the Hamiltonian matrix reads $H = H^0 + H^1$ with

$$H^1_{\mu\in\alpha;\nu\in\beta} = \frac{1}{2}S_{\mu\nu}\sum_\xi^{\text{atoms}}(\Gamma_{\alpha\xi} + \Gamma_{\xi\beta})q_\xi \tag{5}$$

where $\mu \in \alpha$ means that the atomic orbital μ belongs to atom α.

Additional terms can be added to account for London dispersion (E^{disp}) forces as a sum over atomic pairs.[14,78,79] The deMonNano code[80] was used as a starting point to implement these developments.

2.2. Constrained SCC-DFTB. Similarly to the constrained DFT,[63−65] the MOs $\{\phi_i^I\}$, used to build the configuration Φ^I, are obtained from a minimization of the SCC-DFTB energy with the constraints that the charge is carried by fragment I and that the orbitals are orthonormalized. The corresponding Lagrangian is

$$\mathcal{L} = E^{\text{SCC-DFTB}}(\{\phi_i^I\}) + \sum_{ij}\Lambda_{ij}^I(\langle\phi_i^I|\phi_j^I\rangle - \delta_{ij}) + V^I\left(\sum_i n_i\langle\phi_i^I|\hat{P}^I|\phi_i^I\rangle - N^I\right) \tag{6}$$

where V^I is the Lagrange multiplier ensuring the charge localization constraint, $\hat{P}^I$ is the projector of the density on fragment I, N^I is the number of electrons on fragment I, which constrains the charge to be localized on this fragment, and Λ_{ij} represents the Lagrange multipliers ensuring the orbitals' orthonormality constraints. Wu and Van Voorhis[65] discussed the effect of several localization schemes, based on different charge definitions (Mulliken,[81] Löwdin,[82] and Becke's multicenter integration scheme[83]), on the constrained energy, finally using the Löwdin approach. We used for the constrained SCC-DFTB the Mulliken charge definition because (i) the defects of Mulliken charges are less crucial in SCC-DFTB than in DFT due to the use of a minimal atomic basis set (no diffuse functions) and, (ii) in the most used version, SCC-DFTB is a Mulliken charge-based approach, and all of the matrices have been parametrized for this charge definition. This choice leads to the expression for the constraint

$$\sum_{i\nu\mu} n_i c_{i\nu}^I c_{i\mu}^I P_{\nu\mu}^I = N^I \tag{7}$$

with P^I being the projection matrix expressed as[65]

$$P_{\mu\nu}^I = \begin{cases} 0 & \text{if } \mu \notin I \text{ and } \nu \notin I \\ S_{\mu\nu} & \text{if both } \mu \in I \text{ and } \nu \in I \\ \frac{1}{2}S_{\mu\nu} & \text{for other cases } (\mu \in I \text{ or } \nu \in I) \end{cases}$$

The H matrix used in the secular equation (eq 4) becomes

$$H = H^0 + H^1 + V^I P^I$$

Similarly to the constrained DFT, eq 4 must now be solved self-consistently over the atomic charges and contains an unknown Lagrange multiplier V^I. To overcome some convergence problems, we have implemented three ways of solving this equation that can be used alternatively until one of them converges:

(i) The first one (similar to that of ref 63) consists of solving the secular equation with an inner loop and an outer loop. In the inner loop, the Hamiltonian is calculated with a fixed set of atomic charges, and the Lagrange multiplier V^I is modified so that the MOs diagonalizing the Hamiltonian satisfy the charge localization constraint. The outer loop is the self-consistent loop over the atomic charges.

(ii) The second approach consists of inverting the two previous loops; i.e., the inner loop ensures the self-consistence over the Mulliken charges, and the external loop allows the determination of the Lagrange multiplier V^I.

(iii) The third approach is somewhat different and consists of three steps. First, a MOs guess is generated for the isolated fragments. The full set of MOs is orthonormalized with a Löwdin procedure. These MOs do not correspond to an energy minimum and do not satisfy the charge localization constraint. In the second step, the MOs evolve to change charge on fragment I with the iterative procedure:

$$\phi_i^I(n+1) = \phi_i^I(n) + \alpha\left(p^I\phi_i^I(n) + \sum_j \phi_j^I(n)\Lambda_{ij}\right) \quad \forall i \quad (8)$$

where n is the iteration step. The last term ensures the orthonormalization constraint. Transposing this equation in the atomic basis set gives the evolution of the MOs:

$$C^I(n+1) = C^I(n) + \alpha(S^{-1}P^IC^I(n) + XC^I(n)) \quad (9)$$

where $X = \alpha S^{-1}\Lambda$. At each step, the α coefficient is adapted to increase or decrease the charge on fragment I, and the X matrix is calculated solving a second-order equation equivalent to the Rickaert algorithm[84] already implemented for SCC-DFTB Car−Parrinello molecular dynamics.[85] Once a solution satisfying the density constraint is achieved, the last step consists of relaxing the MOs to minimize the energy, under conservation of the charge localization and orthonormality constraints

$$\phi_i^I(n+1) = \phi_i^I(n) + \alpha\left(\frac{dE}{d\phi_i^{I*}} + \sum_j \phi_j^I\Lambda_{ij} + V^IP^I\phi_i^I\right) \quad (10)$$

giving the evolution of the coefficients

$$C^I(n+1) = C^I(n) + \alpha(S^{-1}HC^I(n) + XC^I(n) + V^IS^{-1}P^IC^I(n)) \quad (11)$$

This step requires both the calculation of X and V^I. Starting from a given V^I (the one in the previous step if $n > 1$), $C^I(n+1)$ is determined, calculating X with the Rickaert algorithm. The charge carried by fragment I with these new coefficients is calculated. If this charge is too large (respectively too small), V^I is decreased (respectively increased). The process is repeated until the charge constraint is satisfied. Finally, the MOs converge to the charge-localized solution.

2.3. The Configuration Interaction-Like Scheme. The set of MOs $\{\phi_i^I\}$, obtained from a constrained SCC-DFTB calculation, is used to build the charge-localized configurations Φ^I as single Slater determinants. The coefficients b_I of these configurations in the total wave function Ψ (see eq 1) are obtained by solving the CI-like scheme:

$$\begin{pmatrix} \mathbf{H}_{11} & \mathbf{H}_{12} & .. & \mathbf{H}_{1n} \\ \mathbf{H}_{21} & \mathbf{H}_{22} & .. & \mathbf{H}_{2n} \\ : & : & :: & : \\ \mathbf{H}_{n1} & . & .. & \mathbf{H}_{nn} \end{pmatrix}\begin{pmatrix} b_1 \\ b_2 \\ : \\ b_n \end{pmatrix} = E\begin{pmatrix} \mathbf{S}_1 & \mathbf{S}_{12} & .. & \mathbf{S}_{1n} \\ \mathbf{S}_{21} & \mathbf{S}_2 & .. & \mathbf{S}_{2n} \\ : & : & :: & : \\ \mathbf{S}_{n1} & . & .. & \mathbf{S}_{nn} \end{pmatrix}\begin{pmatrix} b_1 \\ b_2 \\ : \\ b_n \end{pmatrix} \quad (12)$$

where $\mathbf{S}_{IJ}$ is the two-configuration overlap $\langle\Phi^I|\Phi^J\rangle$ and $\mathbf{H}_{II}$ is the energy of the configuration Φ^I already calculated with the constrained SCC-DFTB. Following the approach of Wu et al.,[66,67] the coupling elements $\mathbf{H}_{IJ}$ are calculated by

$$\mathbf{H}_{IJ} = \frac{1}{2}(\mathbf{H}_{II} + \mathbf{H}_{JJ} + N^IV^I + N^JV^J)\mathbf{S}_{IJ} - \frac{1}{2}(V^I\langle\Phi^I|\hat{P}^I|\Phi^J\rangle + V^J\langle\Phi^I|\hat{P}^J|\Phi^J\rangle) \quad (13)$$

In the case of degenerate systems, one can also include more than one configuration to represent the charge localization on a given fragment, as will be shown in the applications of section 3. Solving eq 12 provides both the ground state of the system and some excited states generated via charge resonance. Although these excited states are also of interest, for instance, in spectroscopy, we focus in this work only on the ground state which corresponds to the lowest eigenvalue E_g.

2.4. Analytical Gradients. Derivatives of the energy with respect to atomic nuclear coordinates are required to perform molecular dynamics or geometry optimization. Their numerical calculation is possible by finite differences, but the number of energy calculations ($2 \times 3N_{\text{atoms}}$) turns out to be quite large, even for small systems. Thus, an analytical expression is of primary interest. In SCC-DFTB, it is convenient to use the derivatives of the matrix elements (H^0, S, Γ) which are known and tabulated. Differentiating the constrained SCC-DFTB energy with respect to the nuclear coordinate $\vec{R}_a$ of atom a leads to the force expression

$$\vec{\nabla}_a E_g = \sum_{IJ} b_I b_J(\vec{\nabla}_a\mathbf{H}_{IJ} - E_g\vec{\nabla}_a\mathbf{S}_{IJ}) \quad (14)$$

We now present the calculation of derivatives for the diagonal and off-diagonal elements separately. The differentiation operator $\vec{\nabla}_a$ is replaced by the symbol ∂_a to simplify the expressions.

2.4.1. Derivative of the Diagonal Element. The diagonal element $\mathbf{H}_{II}$ is the energy of the configuration Φ^I. Differentiating the DFTB energy (eq 3 with the dispersion correction terms) and using the eigenvalue equation (eq 4), the molecular charge conservation (eq 7) and orthonormality constraints lead to the analytical expression (see also Wu and Van Voorhis[64]):

$$\partial_a\mathbf{H}_{II} = \partial_aE^{\text{rep}} + \sum_i n_i\sum_{\mu\nu} c_{i\nu}c_{i\mu}(\partial_aH^0_{\mu\nu} + V^I\partial_aP^I_{\mu\nu} + \left(\frac{H^1_{\mu\nu}}{S_{\mu\nu}} - \varepsilon_i\right)\partial_aS_{\mu\nu}) + q_a\sum_b \partial_a\Gamma_{ab}q_b + \partial_aE^{\text{disp}} \quad (15)$$

2.4.2. Derivative of the off-Diagonal Elements. The differentiation of the off-diagonal elements is obtained by differentiating eq 13, namely

$$\partial_a\mathbf{H}_{IJ;I\neq J} = \frac{1}{2}A_{IJ} + \frac{1}{2}A_{JI}$$

with

$$A_{IJ} = (\partial_a \mathbf{H}_{II} + N^I \partial_a V^I)\mathbf{S}_{IJ} + (\mathbf{H}_{II} + N^I V^I)\partial_a \mathbf{S}_{IJ} - \langle \Phi^I | P^I | \Phi^J \rangle \partial_a V^I - V^I \partial_a (\langle \Phi^I | P^I | \Phi^J \rangle) \quad (16)$$

We must now express the derivatives of the Lagrange multiplier $\partial_a V^I$ and those of the overlaps (real overlap and through the projectors) between Φ^I and Φ^J. As there is no relationship between the MOs of the two configurations, there is no Hellman−Feynman type simplification for the derivatives of their overlaps. The analytical derivatives of the orbital coefficients and of the Lagrange multipliers must be explicitly calculated. The derivatives of the coefficients have already been expressed for DFT (see, for instance, ref 86) by solving the coupled perturbed equations. The expression only differs here through the term containing the constraint.

For a given configuration Φ^I, the derivative of the coefficients of the orbitals $\{\phi_i^I\}$ can be related to the orbitals themselves through a u matrix

$$\partial_a c_{i\mu}^I = \sum_k c_{k\mu}^I u_{ki} \quad (17)$$

The conservation of normalized MOs already imposes the form of the diagonal term of the u matrix

$$u_{ii} = -\frac{1}{2} \sum_{\mu\nu} c_{i\mu}^I c_{i\nu}^I \partial_a S_{\mu\nu} \quad (18)$$

For the off-diagonal elements $u_{ij;\, i\neq j}$, differentiating eq 4 leads to

$$u_{ij} = \frac{\partial_a \mathscr{H}_{ij} - \varepsilon_j \partial_a \mathscr{S}_{ij}}{\varepsilon_j - \varepsilon_i} \quad (19)$$

where $\partial_a \mathscr{S}$ and $\partial_a \mathscr{H}$ are the derivatives of the SCC-DFTB overlap and Hamiltonian matrices expressed in the molecular orbital basis set

$$\begin{aligned} \partial_a \mathscr{S}_{ij} &= \sum_{\mu\nu} c_{i\mu}^I c_{j\nu}^I \partial_a S_{\mu\nu} \\ \partial_a \mathscr{H}_{ij} &= \sum_{\mu\nu} c_{i\mu}^I c_{j\nu}^I \partial_a H_{\mu\nu} \end{aligned} \quad (20)$$

In the constrained SCC-DFTB, the Hamiltonian matrix derivatives depend (i) on the derivatives of the matrices H^0, S, Γ, and P; (ii) on the derivatives of the coefficients; and (iii) on the derivatives of the Lagrange multipliers. These three contributions are now explicitly separated:

$$\partial_a \mathscr{H}_{ij} = \partial_a \mathscr{F}_{ij} + \sum_{kl} \mathscr{A}_{ij,kl} u_{lk} + \partial_a V^I \mathscr{P}_{ij} \quad (21)$$

where $\partial_a \mathscr{F}_{ij}$ contains the first contribution

$$\partial_a \mathscr{F}_{ij} = \sum_{\mu\nu} c_{i\mu}^I c_{j\nu}^I \partial_a F_{\mu\nu} \quad (22)$$

with

$$\partial_a F_{\mu\in\alpha,\nu\in\beta} = \partial_a H^0_{\mu\nu} + V^I \partial_a P_{\mu\nu} + \partial_a S_{\mu\nu} \frac{H^1_{\mu\nu}}{S_{\mu\nu}} + \frac{1}{2} S_{\mu\nu} \sum_\xi ((\partial_a \Gamma_{\alpha\xi} + \partial_a \Gamma_{\xi\beta}) q_\xi + \sum_i n_i \sum_l \sum_{\omega\in\xi} (\Gamma_{\alpha\xi} + \Gamma_{\xi\beta}) c_{i\omega} c_{il} \partial_a S_{\omega l})$$

The second term in eq 21 accounts for the Hamiltonian dependences on the orbital coefficients with

$$\mathscr{A}_{ij,kl} = \sum_{\mu\nu} c_{i\mu}^I c_{j\nu}^I \sum_\omega \frac{\partial H_{\mu\nu}}{\partial c_{k\omega}^I} c_{l\omega}^I \quad (23)$$

and

$$\frac{\partial H_{\mu\nu}}{\partial c_{k\omega}^I} = \frac{1}{2} n_k S_{\mu\nu} \sum_\xi \sum_{\lambda\in\xi} S_{\lambda\omega} (\Gamma_{\alpha\gamma} + \Gamma_{\beta\gamma} + \Gamma_{\alpha\xi} + \Gamma_{\beta\xi}) c_{k\lambda}^I \quad (24)$$

where $\mu \in \alpha$; $\nu \in \beta$; $\omega \in \gamma$. In the last term of eq 21, $\mathscr{P}_{ij}$ accounts for the Hamiltonian differentiation upon the Lagrange multiplier

$$\mathscr{P}_{ij} = \sum_{\mu\nu} c_{i\mu}^I c_{j\nu}^I P_{\mu\nu} \quad (25)$$

Compacting the ij indices in a single m index and the kl indices in a single n index, we now define

$$\begin{aligned} u_m &= u_{ij} \\ v_m &= \frac{\partial_a \mathscr{F}_{ij} - \varepsilon_j \partial_a \mathscr{S}_{ij}}{\varepsilon_j - \varepsilon_i} \\ B_{mn} &= \frac{A_{ij,kl}}{\varepsilon_j - \varepsilon_i} \\ w_m &= \frac{\mathscr{P}_{ij}}{\varepsilon_j - \varepsilon_i} \end{aligned}$$

and rewrite eq 19

$$\begin{aligned} u &= Bu + v + \partial_a V^I w \\ &= (1 - B)^{-1} v + \partial_a V^I (1 - B)^{-1} w \\ &= u^0 + \partial_a V^I u' \\ \text{with } u^0 &= (1 - B)^{-1} v \text{ and } u' = (1 - B)^{-1} w \end{aligned} \quad (26)$$

We now determine $\partial_a V^I$ using the fact that N^I remains constant. Differentiating eq 7 leads to

$$\partial_a N^I = \sum_i n_i \sum_{\mu\nu} (c_{i\mu} c_{i\nu} \partial_a P_{\mu\nu} + 2 \partial_a c_{i\mu} c_{i\nu} P_{\mu\nu}) = 0 \quad (27)$$

which can be expressed with the u matrix:

$$\partial_a N^I = \sum_i \sum_{\mu\nu} n_i c_{i\mu} c_{i\nu} \partial_a P_{\mu\nu} + 2 \sum_{ij} n_i u_{ji} \mathscr{P}_{ij} = 0 \quad (28)$$

Using the previous expression for u leads to the following expression for the derivatives of the Lagrange multiplier:

$$\partial_a V^I = -\frac{\sum_i \sum_{\mu\nu} n_i c_{i\mu} c_{i\nu} \partial_a P_{\mu\nu} + 2\sum_{ij} n_i u^0_{ji} \mathscr{P}_{ij}}{2\sum_{ij} n_i u'_{ji} \mathscr{P}_{ij}} \quad (29)$$

$\partial_a \mathscr{H}$ can now be calculated from eq 21, as well as the u matrix from eq 19, and finally the derivatives of the coefficients from eq 17. The $\mathbf{S}_{IJ}$ derivatives are computed from the MO coefficient derivatives and the derivatives of the AO overlap matrix. For sake of efficiency, the determinant expansions appearing in the calculation of the derivatives were calculated using the Sherman−Morrison formula.[87] A similar approach is applied to the derivatives of the projected overlap matrix $\langle \Phi^I | P^I | \Phi^J \rangle$.

Let us mention that, as a check, the analytical gradients have been compared to gradients obtained from finite difference calculations for a set of random geometries. The mean absolute value of forces was 1.4×10^{-2} au with a root-mean-square of 1.8×10^{-2} au, and the mean absolute error was 2.1×10^{-5} au with a root-mean-square of 2.5×10^{-5} au.

2.5. Variant of the DFTB-VBCI: The HOMO Approximation. We will consider the following approximation to the DFTB-VBCI approach: we assume that, in a molecular cluster, the MOs of the different charge localized configurations mostly differ through their Highest Occupied Molecular Orbital (HOMO). The overlaps and projected overlaps between two configurations can then be simplified as

$$\mathbf{S}_{IJ} = \langle \Phi^I | \Phi^J \rangle \simeq \langle \phi^I_{\mathrm{HOMO}} | \phi^J_{\mathrm{HOMO}} \rangle \quad (30)$$

$$\langle \Phi^I | P^I | \Phi^J \rangle \simeq N^I \langle \phi^I_{\mathrm{HOMO}} | \phi^J_{\mathrm{HOMO}} \rangle + \langle \phi^I_{\mathrm{HOMO}} | P^I | \phi^J_{\mathrm{HOMO}} \rangle$$

The off-diagonal CI matrix element becomes

$$\mathbf{H}_{IJ} \simeq \frac{1}{2}(\mathbf{H}_I + \mathbf{H}_J)\langle \phi^I_{\mathrm{HOMO}} | \phi^J_{\mathrm{HOMO}} \rangle - \frac{1}{2}(V^I \langle \phi^I_{\mathrm{HOMO}} | P^I | \phi^J_{\mathrm{HOMO}} \rangle + V^J \langle \phi^I_{\mathrm{HOMO}} | P^J | \phi^J_{\mathrm{HOMO}} \rangle) \quad (31)$$

The advantage of this approach is the ability to avoid any Slater determinant overlap calculation, and only the derivatives of the HOMO coefficients need to be calculated.

3. Applications

We will now apply the DFTB-VBCI method to two prototype cationic molecular clusters, namely, the benzene dimer and the water dimer. All calculations have been performed on a desktop computer (an Intel Xeon 2.8 GHz monoprocessor). Compared with DFTB, the DFTB+VBCI method is more time-consuming. For instance, a single point calculation (without gradients computation) for a water dimer performed over 6×10^{-3} s at the DFTB level takes 0.1 s with the DFTB+VBCI. The single point calculation for the benzene dimer increases from 0.07 s at the DFTB level to 1.67 s at the DFTB+VBCI level. In an optimization procedure, the calculation of the gradient has a small effect on the water dimer (0.14 s per step) but a large effect on the benzene dimer (17 s. per step). Although the computational time is larger than for a simple DFTB calculation, which is the price to pay for treating the charge resonance effects correctly with this method, it remains much lower than high level *ab initio* methods, a typical optimization of about 100 steps for a benzene dimer taking half an hour.

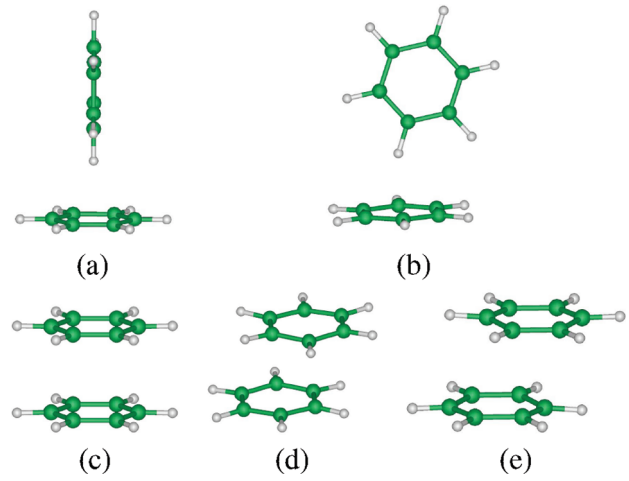

Figure 1. Benzene dimer cations optimized at the DFTB-VBCI level. (a) T-shaped, (b) T_Csob, (c) sandwich stacked, (d) *x*-displaced, and (e) *y*-displaced isomers.

3.1. The Cationic Benzene Dimer. Several authors have investigated cationic benzene dimer clusters at high levels of theory, addressing the relative stability of characteristic isomers, namely, the sandwiches (stacked, parallel *x*- and *y*-displaced) and T-shaped configurations (see Figure 1 and Table 1). Let us cite for instance the work of Miyoshi et al.[88,89] which used a Complete Active Space Self-Consistent Field (CASSCF) followed by a Multi-Reference Coupled Pair Approximation (MRCPA) with a (73/7) basis set decontracted to (721/52) for C and Dunning's DZ set (31) for H. The sandwich parallel displaced isomers were found to be the most stable structures, with binding energies around 12.3 kcal mol^{-1}, more stable than the T-shaped ones by 6.4 kcal mol^{-1}. A similar study was performed by Pieniazeck et al.[90,91] with the Equation-Of-Motion Coupled-Cluster model with Single and Double substitutions for ionized systems (EOM-IP-CCSD/6-31+G*). This calculation yields the same isomer ordering as CASSCF-MRCPA and a similar energy difference between parallel displaced and T-shaped structures. The absolute binding energies are however much higher than for CASSCF-MRCPA (19.58 versus 12.3 kcal mol^{-1} for the *x*-displaced sandwich). In the following, the EOM-IP-CCSD results will be used as references to benchmark our model because (i) the structures have been fully optimized, whereas the CASSCF-MRCPA ones have only been optimized at the CASSCF level, and (ii) the binding energies are in good agreement with the experimental studies, providing values in the 15−20 kcal/mol range.[92−98]

The D_{6h} symmetric stacking is another structure of interest, which is slightly less stable (about 1−2 kcal mol^{-1}) than the two sandwich displaced isomers. We notice that DFT calculations[97,99,100] performed with the B3LYP functional give reasonable binding energies for the sandwich structure (17−19 kcal mol^{-1}) but underestimate the energy difference between the two structures.

Table 1. Binding Energies (kcal/mol) of the Cationic Benzene Dimer Obtained at Different Levels of Theory[a]

	DFTB-VBCI	HOMO Approx.	SCC-DFTB	EOM-IP-CCSD	DFT	CASSCF + MRCPA
stacked sandwich	17.70	17.91	29.53	18.34[b]	18.2[d]−19.1[e]	
x displaced	20.90	20.43	29.01	19.58[c]		12.3[g]
y displaced	21.26	20.79	29.21	19.81[c]	16.57[f]	10.9[g]
T-shaped	9.23	16.90	24.68	12.41[c]	15.7[d]	
T_Csob	9.19	unstable	unstable			

[a] The stacked sandwich structure correspond to constrained D_{6h} optimization whereas the other isomers are fully optimized with the respective methods. [b] Pieniazek et al.[90] [c] Pieniazek et al.[91] [d] Ibrahim et al.[97] [e] Itagaki et al.[99] [f] Kryachko.[100] [g] Miyoshi et al.[89]

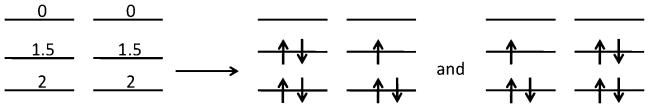

Figure 2. Two electronic configurations (right) obtained from constrained SCC-DFTB calculation with noninteger occupation numbers (left).

Following Pieniazek et al.,[90] we call π_g^a and π_g^o the degenerate MOs in the neutral benzene molecule. In the ionized monomer, these two levels are degenerate at the neutral geometry but undergo Jahn−Teller distortion, leading to an acute angle configuration (ionization from the π_g^a orbital) or an obtuse angle configuration (ionization from the π_g^o orbital). We follow the electronic description of the Dimer Molecular Orbitals Linear Combination from the Fragment Molecular Orbitals (DMO-LCFMO[90]), to describe a benzene dimer, labeling the two fragments A and B. In this framework, the constrained state A^+B can be obtained from removing one electron from either the π_g^a or the π_g^o orbitals of A. Consequently, we need two configurations to describe the constrained form A^+B. In the case of the symmetric D_{6h} sandwich stacked dimer, these two A^+B configurations are degenerate and are built as follows: we use the constrained SCC-DFTB to minimize the electronic energy with an occupation of 1.5 for the two highest occupied MOs (HOMO and HOMO−1) orbitals and 2 for the energetically lower lying orbitals. The two A^+B configurations are then built from the obtained MOs as shown in Figure 2. The same procedure is applied to obtain two AB^+ configurations, and the CI matrix, which has to be diagonalized, is a 4×4 matrix.

In the other isomers (displaced sandwiches and T-shaped), the π_g^a and π_g^o orbitals of each fragment are no longer degenerate, and one could in principle calculate the energy of these configurations without using fractional occupation numbers. However, we could not obtain a self-consistent solution of the A^+B state (respectively AB^+) with the constrained SCC-DFTB since the π_g^a and π_g^o orbitals on fragment A (respectively on B), although not degenerate, remain close in energy. We therefore decided to keep the procedure used for the D_{6h} stacked sandwich isomer, filling the HOMO and HOMO−1 orbitals with 1.5 electrons. Although the filling of the MOs is fixed, these MOs relax anyway and are no longer degenerate in the final results due to the coupling with geometry relaxation. This fractional occupation of the HOMOs would also be usefull to describe the dissociation, keeping the same occupation of the orbitals (see ref 101). Finally, we mention that we use in the empirical dispersion term the parameters of Rapacioli et al.[79] already benchmarked for PAH clusters.

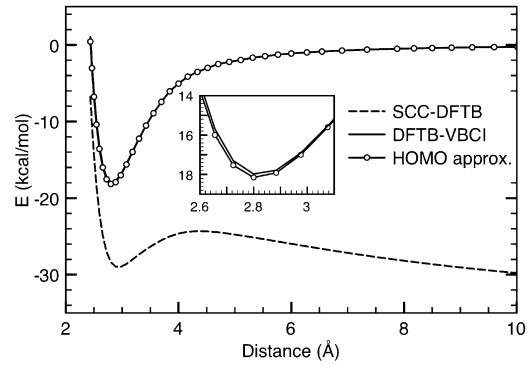

Figure 3. Dissociation potential energy curves of the cationic benzene dimer in the stacked sandwich configuration calculated with SCC-DFTB and DFTB-VBCI approaches.

3.1.1. The Stacked Sandwich Isomer. We first discuss the results obtained for the stacked sandwich in the D_{6h} geometry. Figure 3 represents the energy of the dimer corresponding to the dissociation along the *z* axis, orthogonal to the planes of the monomers. For this example, the fragments are frozen at the monomer neutral geometry. The zero energy reference corresponds to the sum of the separated fragments calculated independently, namely, $E(C_6H_6^+) + E(C_6H_6)$. The SCC-DFTB dissociation curve is reminiscent of the wrong dissociation curve of radical molecules like H_2^+ calculated with DFT (see for instance refs 35 and 36) and can be explained as follows. First, the SCC-DFTB energy does not converge to the sum of the energies of the fragments at the dissociation limit. At infinite distance, the charge is equally distributed over the two fragments. As the evolution of the self-interaction error with the number of electrons on a fragment is unfortunately not constant or linear, we have $2 \times E^{\text{SCC-DFTB}}(C_6H_6^{0.5}) \neq E^{\text{SCC-DFTB}}(C_6H_6^+) + E^{\text{SCC-DFTB}}(C_6H_6)$. At shorter distances, the energy increases, and a barrier is even observed before reaching the minimum, which is here a metastable minimum. The responsible repulsive contribution has a $1/R$ behavior and can be attributed to the artificial repulsion of two half-charged fragments, which is a different kind of self-interaction than the on site one. Finally, the minimum is much too low in energy as compared to the reference calculations (see Table 1). This overstabilization of delocalized states is a well-known effect of the self-interaction error.[102,103]

As can be seen from Figure 3, the DFTB-VBCI method does not present the wrong behavior pattern of the SCC-DFTB curve. At the dissociation limit, the energy converges to the sum of the energies of the fragments. In eq 12, the overlaps and coupling terms vanish, and the energies of the localized configurations are degenerate. These energies are

calculated with the electronic density corresponding to one charged and one neutral monomer and not that of two half-charged fragments. The Coulombic self-interaction $1/R$ repulsion also disappears with this approach, as well as the corresponding barrier. Finally, the binding energy for the stacked sandwich (17.70 kcal/mol) is significantly smaller than the SCC-DFTB one (29.53 kcal/mol) and yields a much better agreement with that of the EOM-IP-CCSD calculation at 18.34 kcal/mol. The interplane distance is 2.84 Å, which is smaller than the 3.3 Å reported at the EOM-IP-CCSD(T) level.[90]

The dissociation curve obtained by applying the HOMO approximation detailed in section 2.5 is also plotted in Figure 3. It is almost identical to the DFTB-VBCI curve with a binding energy of 17.91 kcal/mol vs 17.70 kcal/mol for the DFTB-VBCI.

3.1.2. The T-Shaped and Displaced Sandwich Isomers. The T-shaped and displaced sandwiches have been optimized without any geometrical constraint. The binding energies are reported in Table 1. The T-shaped isomer has a binding energy of 9.23 kcal/mol, which is slightly smaller than the EOM-IP-CCSD one. Another difference concerns the charge localization. With EOM-IP-CCSD, the charge is mostly localized on the stem fragment (88%), whereas its localization drops to 56% with the DFTB-VBCI. A possible explanation for this charge localization discrepancy could be related to some lack of stabilization by polarization. In DFTB-VBCI, the benzene π system can be polarized in the direction parallel to the benzene ring. However, due to the reduced basis set used, the polarization of the π system perpendicular to the benzene ring is underestimated. This lack of polarization could be at the origin of the destabilization of the configuration where the charge is carried by the stem fragment, leading to an oversharing of the charge and an underestimation of the binding energy. Another explanation could rely on the choice of the charge analysis method, which is a NBO analysis for the *ab initio* calculation and Mulliken analysis in the DFTB-VBCI. These two charge definitions are known to produce sometimes different charge distributions even for similar electronic densities. The distance between the centers of the two molecules is 4.52 Å, in good agreement with the EOM-IP-CCSD one (4.59 Å).

In the neutral benzene dimer, the most stable structures have often been reported to be "tilted" T-shaped (also called Cs over atom/bond) configurations.[10,79,104,105] In the cation, the corresponding structures have been reported to be transition states[100] (DFT-B3LYP level). Optimizing the Csob structure at the DFTB-VBCI level leads to a minimum (metastable, 11.7 kcal/mol above the global minimum). The energy difference with the T-shaped structure is smaller than 0.05 kcal/mol, certainly below the accuracy of the method.

At the SCC-DFTB level, the *x*- and *y*-displaced dimers are overstabilized as compared to reference calculations. Similarly to what is observed for the stacked sandwich dimer, the DFTB-VBCI approach gives considerably improved binding energies (20.90 and 21.26 kcal/mol) in very good agreement with those of EOM-IP-CCSD (19.58 and 19.81 kcal/mol). As already found for the D_{6h} benzene case, the interplanar distance is shorter (2.71 and 2.78 Å) compared to EOM-IP-CCSD(T) results (3.08 and 3.18 Å). The sideward shiftings are 1.00 and 1.12 Å, compared to 1.07 (*x*-displaced) and 0.72 (*y*-displaced) Å at the EOM-IP-CCSD(T) level[91] (these shifts are 1.0 Å for both isomers when freezing Jahn−Teller relaxation[90]).

Table 2. Binding Energies (kcal/mol) of Cationic Water Dimer Obtained at Different Levels of Theory

	$[H_2O-H_2O]^+$	$[H_3O-OH]^+$ (C_s)	$[H_3O-OH]^+$ (C_1)
DFTB-VBCI	35.44	42.31	
HOMO Approx.	35.74	42.33	
SCC-DFTB	68.33	47.12	
GGC	53.73[a]	48.66[a]	
BLYP	58.4[b]		49.3[b]
B3LYP	51.5[b]		49.8[b]
MPW1K	42.9[b]		49.9[b]
BH&HLYP	41.4[b]		49.9[b]
MP2	40.48[b]/43.5[c]	50.9[c]	46.47[b]
MP4	41.1[c]	49.9[c]	
CCSD(T)	39.53[b]/39.59[d]	46.64[d]	46.70[b]/46.68[d]
MCPF	36.1[e]	45.9[e]	45.93[e]

[a] Barnett and Landman.[112] [b] Lee and Kim.[111] [c] Gill and Radom.[106] [d] Cheng et al.[110] [e] Sodupe et al.[107] MCPF = SCF + electron correlation included with size extensive Modified-Coupled-Pair Functional.

The two structures are almost degenerate, with a slightly more stable *y*-displaced dimer. The energy difference is however probably much smaller than the expected accuracy of our approach. These are clearly cases in which quantum vibrational effects should be considered.

The global trend when relaxing the geometries compared to neutral dimers is to reduce intermolecular distances. For instance, the interplanar distances in displaced sandwich structures are 2.71/2.78 Å, smaller than those obtained for the neutral dimer (3.39 Å) at the DFTB level.[79] The sideward shifting is also reduced 1.0/1.13 Å versus 1.36 Å in the neutral dimer. The same trend is observed for the T-shaped isomer in which the distance between the molecular centers is reduced from 4.82 to 4.52 Å in the cationic dimer.

Applying the HOMO approximation to the DFTB-VBCI leads to very similar results. The most stable structures are the *x*- and *y*-parallel displaced ones with binding energies differing by less than 2.5% from those of DFTB-VBCI. The T-shaped structure is found to be less stable than the previous isomers, but its binding energy is overestimated as compared to reference calculations and DFTB-VBCI. This suggests that the differences between the charge localized configurations cannot be reduced to a change in the HOMO. We also notice that with this approximation the Csob does not correspond anymore to a minimum, the optimization leading to the T-shaped structure.

3.2. The Cationic Water Dimer. The potential energy surface of cationic water dimers has been investigated using high-level of theories[106−111] (see Table 2). The stable structures belong to two families (Figure 4). In the first one, the two water monomers are superimposed in an antisymmetric pattern, and the charge is equally distributed over the two units. The second one results from a proton transfer leading to two nonsymmetric units $[H_3O-OH]^+$, in which the charge is mostly localized on the H_3O fragment. The structures found to be minima in ref 110

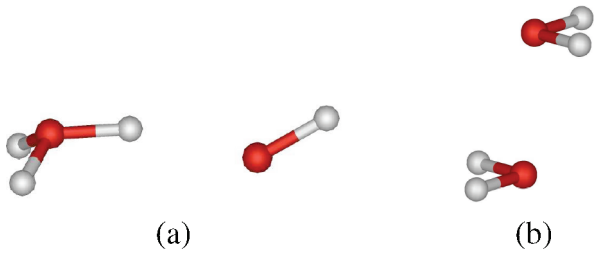

Figure 4. Water dimer cations optimized at the DFTB-VBCI level. (a) $[H_3O-OH]^+$ isomer and (b) $[H_2O-H_2O]^+$ isomer.

have been taken as starts for optimization using the DFTB-VBCI method.

3.2.1. The $[H_3O-OH]^+$ Isomer. Table 2 compares the binding energies obtained at the SCC-DFTB level to those resulting from other calculations. For the $[H_3O-OH]^+$ isomer, most of the DFT functionals (except for the BH&H) give reasonable results as compared to CCSD(T) values. Similarly, the binding energy obtained at the SCC-DFTB level, without CI correction, is close to that of CCSD(T) (47.12 versus 44.6−46.7 kcal mol^{-1}).

In this system, DFTB-VBCI considers the interaction between the configurations where the positive charge is localized either on the H_3O or on the OH fragments. At the dissociation limit, the constrained form (H_3O^+-OH) is obtained by fixing occupation numbers of 1.5 for the two degenerate HOMOs on the neutral OH fragment (in order to maintain the degeneracy of the OH π_x and π_y orbitals), the other occupied orbitals being doubly occupied. The second constrained form (H_3O-OH^+) is obtained with occupation numbers of 0.5 for the two degenerate HOMOs of the neutral H_3O fragment and 0.5 the two degenerate HOMOs on the ionized OH fragment, the other orbitals being doubly occupied. In the complex, the degeneracies are lifted but, similarly to the benzene dimer, we decided to keep these fixed occupation numbers in order to prevent some convergency problems and to have a continuous description of the dissociation, which may be useful in future works.

The weights of the two configurations in the CI approach indicate that the charge is mostly localized (99.9%) on the H_3O fragment. In CCSD(T) calculations, the charge is also strongly localized on this fragment but only by 88% from a restricted open-shell Hartree−Fock level with natural population analysis.[110]

The DFTB-VBCI minimum (C_s-trans) is different from the C_1 minimum obtained with CCSD(T). However, in CCSD(T), the C_s-trans isomer corresponds to a transition state 0.04 kcal/mol higher in energy than the global C_1 minimum[110] (0.1 kcal mol^{-1} for the EOM-IP-CCSD[108] and 0.03 kcal/mol at the SCF+MCPF level[107]). Such a small energy difference is far beyond the expected accuracy of the DFTB-VBCI method. The binding energy of the C_s-trans isomer is close (42.31 kcal/mol) to that obtained with a simple SCC-DFTB calculation (47.12 kcal/mol). This is due to the fact that the charge is not significantly delocalized between the two fragments and that the SCC-DFTB calculation already attributes most of the charge to the H_3O fragment. The artificial stabilization by the self-interaction error is therefore less crucial. This also explains why most of the DFT functionals give reasonable results for this structure. Concerning the geometry, the distance between the two oxygen atoms is 2.66 Å, close to the value of 2.5 Å usually found.[107,108,110,111] The hydrogen bonding is overestimated with 1.74 Å compared to values between 1.44 and 1.47 Å at a high level of calculations.[107,108,110,111]

3.2.2. The $[H_2O-H_2O]^+$ Isomer. It can be seen from Table 2 that, at the CCSD(T) level, the $[H_2O-H_2O]^+$ isomer is less stable by 7 kcal/mol than the $[H_3O-OH]^+$ isomer. At the DFT level, the binding energy strongly depends on the choice of the functional. For instance, the $[H_3O-OH]^+$ structure is more stable than $[H_2O-H_2O]^+$ with MPW1K, BH&H, and BH&LYP functionals, but it is the opposite with the BLYP, BPW91, HCTH407, and B3LYP functionals. At the SCC-DFTB level, the binding energy of the $[H_2O-H_2O]^+$ isomer is strongly overestimated (68 versus 39 kcal mol^{-1} for CCSD(T)), making this isomer 23 kcal/mol more stable than the $[H_3O-OH]^+$ isomer. The DFTB-VBCI leads to a significant improvement, reducing the binding energy to 35.44 kcal/mol, a value close to CCSD(T) results (39 kcal/mol). In this isomer, the charge is equally distributed between the two equivalent fragments. The overstabilization observed at the SCC-DFTB level is attributed to the self-interaction error due to the strong delocalization and is corrected by the DFTB-VBCI approach. This is in line with the fact that self-interaction corrected functionals successfully predict this structure to be less stable by about 8 kcal mol^{-1} than the proton transferred isomer.[108] The distance between the two oxygens is 2.05 Å, in agreement with values between 2.02 and 2.05 Å at higher levels of calculation.[107,108,110,111] We notice that our geometry corresponds to a C_{2h} symmetry, whereas this optimized configuration is often reported in a C_2 geometry (see refs 108, 110, and 111). However, Cheng et al.[110] found that C_2 and C_{2h} structures degenerate at the CCSD(T) level.

Finally, we notice (Table 2) that for both the $[H_3O-OH]^+$ and $[H_2O-H_2O]^+$ isomers, the binding energies obtained with the HOMO approximation are very close to that obtained with the full DFTB-VBCI method.

4. Conclusion

An extended method combining a VBCI-like scheme with SCC-DFTB has been developed. The method has been implemented together with its analytical gradients to enable complete optimization, including the intra- and intermolecular degrees of freedom.

We have benchmarked the DFTB-VBCI approach on the ionized dimers of benzene and water. It is shown for the benzene dimer cation that the self-interaction error is at the origin of the unphysical behavior of the SCC-DFTB dissociation energy curve. It is fully corrected with DFTB-VBCI, as detailed for the stacked sandwich. The binding energies obtained for different isomers with the DFTB-VBCI method agree well with those of high-level calculations as well as experimental data, while these energies are strongly overestimated with SCC-DFTB. We however notice that the main error for the DFTB-VBCI binding energy concerns the T-shaped structure, which is understabilized by 3 kcal/mol. This may be due to the use of point charges and a possible

mistreatment of the multipolar nature of the benzene π system interacting with that of the charged stem benzene. Further improvement of the DFTB-VBCI could include such a multipolar description of the π system as used, for instance, in accurate force field calculations[113] in order to account for this effect but at the price of a larger computational effort to derive the energy gradient.

The second benchmark system is the ionized water dimer. The two lowest energy isomers strongly differ by a proton transfer. The binding energy of the $[H_3O-OH]^+$ isomer calculated at the DFT level with several functionals is in good agreement with reference calculations. This is also the case with SCC-DFTB and DFTB-VBCI due the localization of the charge on the H_3O fragment, reducing the multiconfigurational nature of the wave function and the self-interaction error in standard DFT-based calculations. On the contrary, in the $[H_2O-H_2O]^+$ isomer, the charge is equally carried by the two fragments, and the binding energies obtained at the DFT level strongly differ depending on the choice of the functional. With SCC-DFTB, this structure is overstabilized and becomes artificially the most stable one. This effect is corrected with the DFTB-VBCI approach, which gives a binding energy close to that of high-level calculations.

For the two benchmark systems, the binding energies are in quantitative agreement with those of higher levels of calculation. Concerning the geometries, some differences have been observed with those of high level calculations, the most critical one being the interplane distance in benzene sandwich structures. This could be due to the reduced basis used in DFTB leading to an underestimation of overlaps and consequently charge resonance stabilization at large distances. Neglecting the three body integrals in the DFTB could also play a role, which is difficult to estimate.

In this work, we have been concerned with the analytical derivation of the gradients, and optimizing the efficiency of the code will be a further step. One of the key computational difficulties is the double SCF involving both the charge and constraint. Efficiency could certainly be strongly improved by using extrapolation schemes of the Lagrangian parameter and atomic charges (Broyden[114] or Pulay[115] schemes) also transferring the SCF densities from one geometry to the next one. In the gradient computation, most of the time is spent in the calculation of the inverse of the *A* matrix, which could be calculated iteratively. Starting from the inverse of *A* calculated at the previous step would reduce the number of iterations. All of these improvements would of course not affect the accuracy of the method.

Beyond molecular clusters, the direct applicability of the method to the fragmentation of organometallic complexes might be less straightforward. The present scheme requires an *a priori* identification of the ligand metal partition, which may not be unique; then one possibility could be to use small-scale fragments, for instance, one per ligand. The present scheme has been applied to cationic systems. Dealing with the localization/delocalization process in anionic molecular clusters could be considered with a simillar scheme. However, the treatment of the molecular negative units is not very reliable since DFTB is expressed in a minimal valence basis, while the description of molecular anions even with DFT generally requires extended basis sets with diffuse functions and even sometimes very diffuse functions for describing dipole- and quadrupole-bound anions.

We now plan to perform global explorations of the potential energy surfaces through molecular dynamics or Monte Carlo sampling with the aim of studying ionized dimer dissociation. When the advantage of SCC-DFTB in terms of computational efficiency is taken, the DFTB-VBCI will allow for dealing with systems much larger than dimers. In our previous study, DFTB-VBCI has been used to characterize binding energies, ionization potentials, as well as charge localization in stacked coronene clusters with frozen intramolecular geometries and equal spacings between the units.[77] This preliminary work was however performed before the development of the analytical nuclear gradients, and it will be of interest to characterize the effects of intra- and intermolecular relaxation in these clusters. As for the hole delocalization, one could expect similar patterns as those of the rare gas clusters He_n^+, Ne_n^+, Ar_n^+, Kr_n^+, and Xe_n^+, for which the hole tends to delocalize on a few units (from 2 to 4, depending on the rare gas) and the other atoms tend to organize in crowns around a linear core.[116] We plan to investigate how the monomer internal degrees of freedom, the molecular extension, and the shape influence the size of the core unit and the general organization in molecular clusters with polyatomic monomers. Another perspective will be to study charge dynamics in such clusters, which is possible since the model also provides charge transfer excited states.

Acknowledgment. The authors would like to acknowledge the cluster research group GDR 2758 for its support and the supercomputing facility of Toulouse III University, CALMIP, for generous allocation of computer resources.

Supporting Information Available: Optimized geometries of cationic molecular dimers. This material is available free of charge via the Internet at http://pubs.acs.org.

References

(1) Zhao, Y.; Schultz, N. E.; Truhlar, D. G. *J. Chem. Phys.* **2005**, *123*, 161103–4.

(2) Dion, M.; Rydberg, H.; Schröder, E.; Langreth, D. C.; Lundqvist, B. I. *Phys. Rev. Lett.* **2004**, *92*, 246401–4.

(3) Sato, T.; Tsuneda, T.; Hirao, K. *J. Chem. Phys.* **2005**, *123*, 104307–10.

(4) Sato, T.; Tsuneda, T.; Hirao, K. *J. Chem. Phys.* **2007**, *126*, 234114–12.

(5) Langreth, D. C.; Dion, M.; Rydberg, H.; Schroder, E.; Hyldgaard, P.; Lundqvist, B. I. *Int. J. Quantum Chem.* **2005**, *101*, 599–610.

(6) Chakarova-Kack, S. D.; Schroder, E.; Lundqvist, B. I.; Langreth, D. C. *Phys. Rev. Lett.* **2006**, *96*, 146107–4.

(7) Thonhauser, T.; Cooper, V. R.; Li, S.; Puzder, A.; Hyldgaard, P.; Langreth, D. C. *Phys. Rev. B* **2007**, *76*, 125112–11.

(8) von Lilienfeld, O. A.; Tavernelli, I.; Rothlisberger, U.; Sebastiani, D. *Phys. Rev. Lett.* **2004**, *93*, 153004–4.

(9) Zhao, Y.; Truhlar, D. G. *J. Phys. Chem. A* **2004**, *108*, 6908–6918.

(10) Gräfenstein, J.; Cremer, D. *J. Chem. Phys.* **2009**, *130*, 124105–16.

(11) Lewis, J. P.; Sankey, O. F. *Biophys. J.* **1995**, *69*, 1068–1076.

(12) Meijer, E. J.; Sprik, M. *J. Chem. Phys.* **1996**, *105*, 8684–8689.

(13) Gianturco, F. A.; Paesani, F.; Laranjeira, M. F.; Vassilenko, V.; Cunha, M. A. *J. Chem. Phys.* **1999**, *110*, 7832–7845.

(14) Elstner, M.; Hobza, P.; Frauenheim, T.; Suhai, S.; Kaxiras, E. *J. Chem. Phys.* **2001**, *114*, 5149–5155.

(15) Wu, Q.; Yang, W. *J. Chem. Phys.* **2002**, *116*, 515–524.

(16) Zimmerli, U.; Parrinello, M.; Koumoutsakos, P. *J. Chem. Phys.* **2004**, *120*, 2693–2699.

(17) Grimme, S. *J. Comput. Chem.* **2004**, *25*, 1463–1473.

(18) Goursot, A.; Mineva, T.; Kevorkyants, R.; Talbi, D. *J. Chem. Theory Comput.* **2007**, *3*, 755–763.

(19) Perdew, J. P.; Zunger, A. *Phys. Rev. B* **1981**, *23*, 5048–5079.

(20) Pederson, M. R.; Heaton, R. A.; Lin, C. C. *J. Chem. Phys.* **1985**, *82*, 2688–2699.

(21) Krieger, J. B.; Li, Y. *Phys. Rev. A* **1989**, *39*, 6052–6055.

(22) Johnson, B. G.; Gonzales, C. A.; Gill, P. M. W.; Pople, J. A. *Chem. Phys. Lett.* **1994**, *221*, 100–108.

(23) Ruiz, E.; Salahub, D. R.; Vela, A. *J. Phys. Chem.* **1996**, *100*, 12265–12276.

(24) Goedecker, S.; Umrigar, C. J. *Phys. Rev. A* **1997**, *55*, 1765–1771.

(25) Baerends, E. J.; Gritsenko, O. V. *J. Phys. Chem. A* **1997**, *101*, 5383–5403.

(26) Csonka, G. I.; Johnson, B. G. *Theor. Chem. Acc.* **1998**, *99*, 158–165.

(27) Chermette, H.; Ciofini, I.; Mariotti, F.; Daul, C. *J. Chem. Phys.* **2001**, *115*, 11068–11079.

(28) Garza, J.; Vargas, R.; Nichols, J. A.; Dixon, D. A. *J. Chem. Phys.* **2001**, *114*, 639–651.

(29) Della Sala, F.; Gorling, A. *J. Chem. Phys.* **2001**, *115*, 5718–5732.

(30) Patchkovskii, S.; Ziegler, T. *J. Phys. Chem. A* **2002**, *106*, 1088–1099.

(31) Polo, V.; Gräfenstein, J.; Kraka, E.; Cremer, D. *Chem. Phys. Lett.* **2002**, *352*, 469–478.

(32) Polo, V.; Kraka, E.; Cremer, D. *Mol. Phys.* **2002**, *100*, 1771–1790.

(33) Polo, V.; Gräfenstein, J.; Kraka, E.; Cremer, D. *Theor. Chem. Acc.* **2003**, *109*, 22–35.

(34) Kummel, S.; Perdew, J. P. *Mol. Phys.* **2003**, *101*, 1363–1368.

(35) Gräfenstein, J.; Kraka, E.; Cremer, D. *J. Chem. Phys.* **2004**, *120*, 524–539.

(36) Gräfenstein, J.; Kraka, E.; Cremer, D. *Phys. Chem. Chem. Phys.* **2004**, *6*, 1096–1112.

(37) Ciofini, I.; Adamo, C.; Chermette, H. *Chem. Phys.* **2005**, *309*, 67–76.

(38) Dinh, P. M.; Messud, J.; Reinhard, P. G.; Suraud, E. *Phys. Lett. A* **2008**, *372*, 5598–5602.

(39) Duch, W. *J. Mol. Struct. Theochem* **1991**, *234*, 27–49.

(40) Siegbahn, P. E. M. *The Configuration Interaction Method in Lecture Notes in Chemistry*; Roos, B. O., Eds.; Springer Verlag: New York, 1992; Volume *58*, pp 255−293.

(41) Roos, B. O. *The Multiconfigurational (MC) Self-Consistent Field (SCF) Theory in Lecture Notes in Chemistry*; Roos, B. O., Eds.; Springer Verlag: New York, 1992; Volume *58*, pp 177−254.

(42) Werner, H.-J. *Adv. Chem. Phys.* **1987**, *69*, 1.

(43) Bartlett, R. J. *Coupled-Cluster Theory: An Overview of Recent Developments*; Yarkony, D. R., Eds.; World Scientific: Singapore, 1995; pp 1047−1131.

(44) Helgaker, T.; Jorgensen, P.; Olsen, J. *Molecular Electronic Structure Theory*; Wiley & Sons: New York, 2000; pp 140−200.

(45) Savin, A. *Recent developments and applications of modern Density Functional Theory*; Seminario, J., Eds.; Elsevier: Amsterdam, 1996; pp 327−357.

(46) Leininger, T.; Stoll, H.; Werner, H.-J.; Savin, A. *Chem. Phys. Lett.* **1997**, *275*, 151–160.

(47) Goll, E.; Werner, H.-J.; Stoll, H. *Phys. Chem. Chem. Phys.* **2005**, *7*, 3917–3923.

(48) Goll, E.; Werner, H. J.; Stoll, H. *Chem. Phys.* **2008**, *346*, 257–265.

(49) Møller, C.; Plesset, M. S. *Phys. Rev.* **1934**, *46*, 618–622.

(50) Werner, H.-J.; Manby, F. R.; Knowles, P. J. *J. Chem. Phys.* **2003**, *118*, 8149–8160.

(51) Schutz, M.; Werner, H.-J.; Lindh, R.; Manby, F. R. *J. Chem. Phys.* **2004**, *121*, 737–750.

(52) Heitler, W.; London, F. *Z. Phys.* **1927**, *44*, 455–472.

(53) Pauling, L. *The Nature of the Chemical Bond*; Cornell University Press: New York, 1939; pp 183−220.

(54) Murrell, J.-N.; Kettle, S.; Tedder, J. *The Chemical Bond*; John Wiley & Sons: Chichester, U. K., 1985; pp 1−60.

(55) Shaik, S. S.; Hiberty, P. C. *A Chemist's Guide to Valence Bond Theory*; Wiley-Interscience: New Jersey, 2008; pp 1−290.

(56) Vragović, I.; Scholz, R. *Phys. Rev. B* **2003**, *68*, 155202–16.

(57) Bouvier, B.; Brenner, V.; Millié, P.; Soudan, J.-M. *J. Phys. Chem. A* **2002**, *106*, 10326–10341.

(58) Amarouche, M.; Durand, G.; Malrieu, J. P. *J. Chem. Phys.* **1988**, *88*, 1010–1018.

(59) Durand, G.; Spiegelman, F. *Theor. Chem. Acc.* **2006**, *116*, 549–558.

(60) Grigorov, M.; Spiegelman, F. *Surf. Rev. Lett.* **1996**, *3*, 211–215.

(61) Calvo, F.; Galindez, J.; Gadea, F. X. *Phys. Chem. Chem. Phys.* **2003**, *5*, 321–328.

(62) Calvo, F.; Bonhommeau, D.; Parneix, P. *Phys. Rev. Lett.* **2007**, *99*, 083401−4.

(63) Wu, Q.; Van Voorhis, T. *Phys. Rev. A* **2005**, *72*, 024502−4.

(64) Wu, Q.; Van Voorhis, T. *J. Phys. Chem. A* **2006**, *110*, 9212–9218.

(65) Wu, Q.; Van Voorhis, T. *J. Chem. Theory Comput.* **2006**, *2*, 765–774.

(66) Wu, Q.; Cheng, C.-L.; Van Voorhis, T. *J. Chem. Phys.* **2007**, *127*, 164119–9.

(67) Wu, Q.; Van Voorhis, T. *J. Chem. Phys.* **2006**, *125*, 164105–9.

(68) Wu, Q.; Kaduk, B.; Van Voorhis, T. *J. Chem. Phys.* **2009**, *130*, 034109−7.

(69) Van Voorhis, T.; Kowalczyk, T.; Kaduk, B.; Wang, L.-P.; Cheng, C.-L.; Wu, Q. *Annu. Rev. Phys. Chem.* **2010**, *61*, 149–170.

(70) Roos, B. O. *Advances in Chemical Physics; Ab Initio Methods in Quantum Chemistry - II*; Lawley, K. P., Eds.; Wiley & Sons: Chichester, U. K., 1987; Volume *69*, pp 399−445.

(71) Werner, H. J. *Mol. Phys.* **1996**, *89*, 645.

(72) Porezag, D.; Frauenheim, T.; Köhler, T.; Seifert, G.; Kaschner, R. *Phys. Rev.B* **1995**, *51*, 12947–12957.

(73) Seifert, G.; Porezag, D.; Frauenheim, T. *Int. J. Quantum Chem.* **1996**, *58*, 185.

(74) Elstner, M.; Porezag, D.; Jungnickel, G.; Elsner, J.; Haugk, M.; Frauenheim, T.; Suhai, S.; Seifert, G. *Phys. Rev. B* **1998**, *58*, 7260–7268.

(75) Oliveira, A.; Seifert, G.; Heine, T.; duarte, H. *J. Braz. Chem. Soc.* **2009**, *20*, 1193–1205.

(76) Gräfenstein, J.; Cremer, D. *Theor. Chem. Acc.* **2009**, *123*, 171–182, 10.1007/s00214−009−0545−9.

(77) Rapacioli, M.; Spiegelman, F. *Eur. Phys. J. D* **2009**, *52*, 55–58.

(78) Zhechkov, L.; Heine, T.; Patchovskii, S.; Seifert, G.; Duarte, H. *J. Chem. Theory Comput.* **2005**, *1*, 841–847.

(79) Rapacioli, M.; Spiegelman, F.; Talbi, D.; Mineva, T.; Goursot, A.; Heine, T.; Seifert, G. *J. Chem. Phys.* **2009**, *130*, 244304–10.

(80) Heine, T.; Rapacioli, M.; Patchkovskii, S.; Frenzel, J.; Koster, A.; Calaminici, P.; Duarte, H. A.; Escalante, S.; Flores-Moreno, R.; Goursot, A.; Reveles, J.; Salahub, D.; Vela, A. deMon-Nano Experiment 2009. http://physics.jacobs-university.de/theine/research/deMon/ (accessed Nov 2010).

(81) Mulliken, R. S. *J. Chem. Phys.* **1955**, *23*, 1833–1840.

(82) Lowdin, P.-O. *J. Chem. Phys.* **1950**, *18*, 365–375.

(83) Becke, A. D. *J. Chem. Phys.* **1988**, *88*, 2547–2553.

(84) Ryckaert, J.; Cicotti, G.; Berendsen, H. *J. Comput. Phys.* **1977**, *23*, 327–341.

(85) Rapacioli, M.; Barthel, R.; Heine, T.; Seifert, G. *J. Chem. Phys.* **2007**, *126*, 124103–7.

(86) Wolff, S. *Int. J. Quantum Chem.* **2005**, *104*, 645–659.

(87) Hager, W. W. *SIAM Rev.* **1989**, *31*, 221–239.

(88) Miyoshi, E.; Ichikawa, T.; Sumi, T.; Sakai, Y.; Shida, N. *Chem. Phys. Lett.* **1997**, *275*, 404–408.

(89) Miyoshi, E.; Yamamoto, N.; Sekiya, M.; Tanaka, K. *Mol. Phys.* **2003**, *101*, 227–232.

(90) Pieniazek, P. A.; Krylov, A. I.; Bradforth, S. E. *J. Chem. Phys.* **2007**, *127*, 044317−16.

(91) Pieniazek, P. A.; Bradforth, S. E.; Krylov, A. I. *J. Chem. Phys.* **2008**, *129*, 074104−11.

(92) Field, F. H.; Hamlet, P.; Libby, W. F. *J. Am. Chem. Soc.* **1969**, *91*, 2839–2842.

(93) Grover, J. R.; Walters, E. A.; Hui, E. T. *J. Phys. Chem.* **1987**, *91*, 3233–3237.

(94) Krause, H.; Ernstberger, B.; Neusser, H. J. *Chem. Phys. Lett.* **1991**, *184*, 411–417.

(95) Meot-Ner, M.; Hamlet, P.; Hunter, E. P.; Field, F. H. *J. Am. Chem. Soc.* **1978**, *100*, 5466–5471.

(96) Hiraoka, K.; Fujimaki, S.; Aruga, K.; Yamabe, S. *J. Chem. Phys.* **1991**, *95*, 8413–8418.

(97) Ibrahim, Y.; Alsharaeh, E.; Rusyniak, M.; Watson, S.; Mautner, M. M. N.; El-Shall, M. S. *Chem. Phys. Lett.* **2003**, *380*, 21–28.

(98) Rusyniak, M.; Ibrahim, Y.; Alsharaeh, E.; Meot-Ner (Mautner), M.; El-Shall, M. *J. Phys. Chem. A* **2003**, *107*, 7656–7666.

(99) Itagaki, Y.; Benetis, N. P.; Kadam, R. M.; Lund, A. *Phys. Chem. Chem. Phys.* **2000**, *2*, 2683–2689.

(100) Kryachko, E. S. *Int. J. Quantum Chem.* **2007**, *107*, 2741–2755.

(101) Nesbet, R. K. *Proc. R. Soc. London* **1955**, *A230*, 312–321.

(102) Bally, T.; Sastry, G. N. *J. Phys. Chem. A* **1997**, *101*, 7923–7925.

(103) Lundberg, M.; Siegbahn, P. E. M. *J. Chem. Phys.* **2005**, *122*, 224103–9.

(104) Podeszwa, R.; Bukowski, R.; Szalewicz, K. *J. Phys. Chem. A* **2006**, *110*, 10345–10354.

(105) Lee, E. C.; Kim, D.; Jurecka, P.; Tarakeshwar, P.; Hobza, P.; Kim, K. S. *J. Phys. Chem. A* **2007**, *111*, 3446–3457.

(106) Gill, P. M. W.; Radom, L. *J. Am. Chem. Soc.* **1988**, *110*, 4931–4941.

(107) Sodupe, M.; Oliva, A.; Bertran, J. *J. Am. Chem. Soc.* **1994**, *116*, 8249–8258.

(108) Pieniazek, P. A.; VandeVondele, J.; Jungwirth, P.; Krylov, A. I.; Bradforth, S. E. *J. Phys. Chem. A* **2008**, *112*, 6159–6170.

(109) Periyasamy, G.; Levine, R. D.; Remacle, F. *Chem. Phys.* **2009**, *366*, 129–138.

(110) Cheng, Q.; Evangelista, F. A.; Simmonett, A. C.; Yamaguchi, Y.; Schaefer, H. F. *J. Phys. Chem. A* **2009**, *113*, 13779–13789.

(111) Lee, H. M.; Kim, K. S. *J. Chem. Theory Comput.* **2009**, *5*, 976–981.

(112) Barnett, R. N.; Landman, U. *J. Phys. Chem.* **1995**, *99*, 17305–17310.

(113) Piquemal, J.-P.; Gresh, N.; Giessner-Prettre, C. *J. Phys. Chem. A* **2003**, *107*, 10353–10359.

(114) Broyden, C. *Math. Comput.* **1965**, *19*, 577–593.

(115) Pulay, P. *J. Comput. Chem.* **1982**, *3*, 556–560.

(116) Haberland, H.; von Issendorff, B.; Kolar, T.; Kornmeier, H.; Ludewigt, C.; Risch, A. *Phys. Rev. Lett.* **1991**, *67*, 3290–3293.

CT100412F